The effect of graphene layers on the growth of vanadium oxide nanostructures: Structural, morphological and optical investigations and mechanisms revelation

Issam Derkaoui[1,3], Mohammed Khenfouch[2,3*], Ibrahim Elmokri[1], Bakang M. Mothudi[2], Mokhotjwa S. Dhlamini[2], Sabata J. Moloi[2]. Anouar Jorio[1], Izeddine Zorkani[1], Malik Maaza[4,5]

[1]University Sidi Mohammed Ben Abdellah, Faculty of Sciences Dhar el Mahraz, Laboratory of Solid state Physics, Group of Nanomaterials and Renewable Energies, PO Box 1796 Atlas Fez, 30000, Morocco
[2]University of South Africa, Department of Physics, College of Science, Engineering and Technology, Science Campus, Cnr Christiaan de Wet & Pioneer Avenue Florida 1709, Johannesburg, South Africa
[3]Africa Graphene Center, 2 Boekenhout street, Florida, Johannesburg, 1709, South Africa
[4]Nanosciences African Network (NANOAFNET), iThemba LABS-National Research Foundation, 1 Old Faure Road, Somerset West 7129, PO Box 722, Somerset West, Western Cape-South Africa
[5]UNESCO-UNISA Africa Chair in Nanosciences Nanotechnology, College of Graduate Studies, University of South Africa, Muckleneuk ridge, PO Box 392, Pretoria - South Africa

[*]Corresponding author. Tel: (+27) 742368876; E-mail: khenfouch@yahoo.fr

Received: 03 October 2016, Revised: 11 November 2016 and Accepted: 16 December 2016

DOI: 10.5185/amlett.2017.1440
www.vbripress.com/aml

Abstract

Most recently, Vanadium oxide nanoparticles/reduced Graphene oxide (VO-NPs/rGO) nanocomposite have attracted extensive attention due to their potential applications in energy-related areas. Hence, understanding the interactions on behalf the effect of graphene layers on the modification of VO-NPs properties as well as their growth mechanism are of great importance. In this work, our results are revealing that VO-NPs were efficiently grown and coated on the graphene surface and are clearly showing the strong effect of rGO layers on the growth of VO-NPs which leads to a modification in the form, the shape and also the phase. These interactions which were studied based on structural and morphological investigations will play an important role on the modification of these nanocomposites properties which is suitable for a wide range of potential applications and particularly as electrode in Li-ion batteries. Copyright © 2017 VBRI Press.

Keywords: Vanadium oxide, graphene, growth mechanism, nanocomposites.

Introduction

Graphene, a two-dimensional (2D) layer of sp^2-bonded carbon material with very unique physical and chemical properties, high electrical conductivity, flexibility and large surface area (theoretical value of 2630 m^2 g^{-1}) has been explored as an ideal matrix to host nanomaterials **[1]**. In addition, these unique outstanding physicochemical properties depend strongly on the number of layers and the dispersion performance of graphene sheets **[2]**. Furthermore, these promising properties have caused researchers and companies to consider using this material in several fields for different technologies including photovoltaics, nanoelectronics, spintronics and energy storage **[3]**.

One-dimensional nanostructures with different morphologies, such as nanorods, nanowires, nanotubes and nanobelts, have attracted considerable attentions because to both their wide range of oxidation states (from +2 to +5) in the vanadium-oxygen system **[4]** and specific physical and chemical properties that are different from the bulk materials due to their limited size and high density of corner or edge surface sites **[5]**. Owing to their important properties they exhibit potential application in fabricating nanoscale electronic, optical, electrochemical, optoelectronic, and electromechanical devices **[6, 7]**. Because of these attractive properties and applications, various preparation methods of VO-NPs have been developed such as chemical vapor deposition **[8]**, sol-gel **[9]**, solution-based method **[10]**, thermolysis **[11]**, pulsed laser ablation **[12]**.

Up to now, carbon matrices such as graphite, carbon Black and carbon nanotubes have been widely chosen to improve the electrode conductivities (ECs) and stabilities **[13]**. Compared with other carbon matrices, graphene is emerging as one of the most appealing materials because of its unique properties **[14]**. Moreover, the development of graphene-based composites provides an important milestone. The hybridization of metal or semiconductor nanoparticles with graphene has been demonstrated to be

an effective strategy for improved the electrochemical performance of electrode materials **[15]**. With this in mind, considerable efforts of decorating graphene with metal oxides NPs have recently been reported because of the synergetic effect between them **[16]**, which leads to increase the stability were graphene acts as a buffer layer and anchoring of this nanoparticles onto graphene sheets prevents aggregation and loss of surface area **[17]**.

Graphene-Vanadium oxide composites have attracted extensive attention for their potential applications in energy-related areas **[18, 19]**. They are a novel and one of the most attractive anodes in energy storage applications **[20]**, so the hybrid ribbons of vanadium oxide and graphene may accelerate the development of high-power lithium-ion batteries suitable for many demanding applications **[21]**. Hence, understanding the interactions which lead to this improvement as well as the growth mechanism is of great importance. Many synthesis methods solutions based method, sol-gel, chemical vapor deposition, hydrothermal and several ones were used to synthesize graphene-Vanadium oxides composites. Therefore, the hydrothermal method for is particularly successful in terms of controlling the chemical composition, particle shape, and crystallite size in a simple and inexpensive way **[22, 23]**.

To the best of our knowledge, this is the first study of the effect of graphene nanosheets on the structural properties. our result highlighted the modification of VO-NPs form, shape and phase after the introduction of graphene nanosheets, which is confirmed firstly by transfer from nanobelt vanadium oxide to nanorods like shape. Secondly, revealing the coexistence of three phases H_2VO_3, VO_2 and V_6O_{13} starting only from two phases V_4O_7 and VO_2. The use of these nancomposites is promising way for the development of technological applications especially for energy storage devices as lithium-ion batteries **[20, 21]**

In this work, in order to understand the effects of the graphene layers on the growth of vanadium oxide nanoparticles, we are presenting a structural study of these hybrids, which include growth mechanism description and interactions discussion. It is revealing that vanadium oxide nanobelts were efficiently grown and had nanorods like shape in the presence of graphene. In this sense, transmission electron microscopy (TEM), X-ray diffraction (XRD), Raman Spectroscopy and Ultraviolet-visible absorbance spectra (Uv-Vis) were investigated.

Experimental

Material preparation

In a typical procedure, commercial V_2O_5 powder (0,45g) sulphuric acid, H_2SO_4, (0.75 ml), and H_2O (0, 5 ml) were vigorously stirred in room atmosphere for 20 min, then an orange suspension was obtained. The obtained suspension was followed by the addition of N_2H_4-$2H_2O$. After stirring thoroughly, the solution color changed from orange (V^{5+} valence state) to blue, indicating the reduction of V^{5+} to yield V^{4+} ions. In this case, hydrazine was still necessary for the formation of vanadium oxide nanoparticles. Heat could also be applied to the solution while adding NaOH solution. A gray to brown precipitate formed during the addition of NaOH solution. The pH of the resultant strongly acidic blue VO^{2+} solution was then close to 5 by adding NaOH solution. Afterward, the suspension was transferred into a 25 mL Teflon-lined stainless autoclave. The autoclave was maintained at 230 °C for 48 h and then air cooled to room temperature. The resulting dark blue precipitates were collected and washed several times with distilled water and ethanol and then dried at 60°C under vacuum for few hours. Graphene oxide nanosheets were synthesized from pure graphite using $KMnO_4$ and H_2SO_4 according to the modified Hummer's method **[24]**, then chemical reduction was occurred using hydrazine as reducing agent with stirring for 6 h at 40°C to produce reduced graphene oxide **[25, 26]**. Finally, VO-NPs/rGO nanocomposites (1:1 in molar ratio) were prepared by adding graphene suspension to the prepared vanadium oxide nanoparticles solution before running the hydrothermal process.

Material characterization

To characterize the obtained samples, TEM images were employed to analyze the morphology of rGO, VO-NPs and VO-NPs/rGO nanocomposite. XRD pattern were obtained from a Rigaku Smart Lab system using Cu Kα (λ=1.54178 $\mathring{A}$), Raman spectra were obtained using a Bruker Multi Ram with and excitation wavelength of 1064 nm. Finally, Ultraviolet-visible absorbance spectra were carried out using Perkin Elmer lambda 1050 UV/Vis/NIR spectrometer.

Growth mechanism

Vanadium oxides can be selectively synthesized with controllable phase structures under controlled hydrothermal conditions. For example, there is a definite phase progression V_2O_5, $V_3O_7.H_2O$, VO_2(B), VO_2(A) and VO_2(M) with increasing hydrothermal time or temperature. First, V_2O_5 and H_2SO_4 were mixed to form $VOSO_4$ which will lead to the production of VO^{2+} ions after its reduction following the reactions below:

$$H_2SO_4 + V_2O_5 \longrightarrow VOSO_4 \quad (1)$$

$$VOSO_4 + N_2H_4 + H_2O \longrightarrow VO^{2+} + 2e^- + N_2H_6SO_4 \quad (2)$$

By adding hydrazine and NaOH solution to VO^{2+} solution, the reaction was producing a gray-brown hydrous precipitate, which is probably a complex of VO^{2+}, OH^-, and hydrazine. Then, two reactions may occur to form, a two-electron reduction leading to V^{2+} and a one-electron oxidation leading to VO^{2+}. The redox potential for the vanadium half-reaction is given by:

$$VO^{2+} + H_2O \longrightarrow VO_2^+ + 2H^+ + e^- \quad (3)$$

VO-NPs nucleation starts hydrothermally when VO^{2+} and OH^- reach the critical value of the super-saturation of VO OH^- and forms $VO(OH)_2$, the growth units of VO-NPs as described by the following reactions:

$$VO_2^+ + 2OH^- \longrightarrow VO(OH)_2(s) \quad (4)$$

$$VO(OH)_2(s) \longrightarrow V_xO_y(s) + H_2O \quad (5)$$

In this step, the synthesized VO-NPs had nanobelt like shape. To clarify, The overall reaction conditions, crystal phases, and product morphologies of VO-NPs nanobelts and other works by Son et al **[27]** and Zhang et al **[28]** are summarized in **Tables 1**. The reaction conditions such as pH, concentration, and temperature during the formation of vanadium oxides nanoparticles were important factors in determining the size and shape of the final product.

For the nanocomposite, $VO(OH)_2$, the growth units of vanadium oxide, start to be attached on top of the seed layer (graphene sheet in our case), then they became VO-NPs nanoparticles. If the growth was not stopped electronically, which produce CO bonds, and/or mechanically, by the deposition of graphene sheets on the top of those nanoparticles, they will continue growing to form nanobelts where the growth conditions have a great influence on the formation of the final synthesized material **(Fig. 1)**. In our solution, The size and the morphology of those nanostructures will vary from one region to another depending on the nature and the concentration of ions incorporated between graphene sheets which will give birth to nanoparticles, nanorods or even non dissolved $VO(OH)_2$.

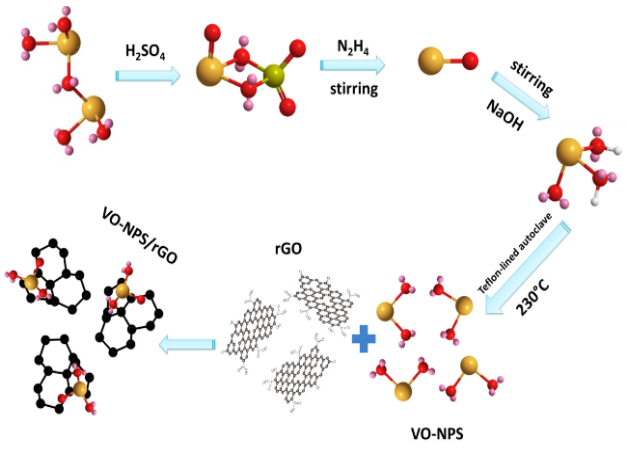

Fig. 1. Growth mechanism of VO-NPs/rGO nanocomposite.

Table 1. Comparison between Synthesis conditions, crystal phases, Sizes and morphologies of the as-synthesized vanadium oxides nanoparticles nanobelts [a] and the literature **[27, 28]**.

V_2O_5(g)	H_2SO_4(ml)	$N_2H_4.2H_2O$(ml)	T (°C)	NaOH	pH	reaction condition	size	VO-NPs (%)
0.45	0.75	0.175	60	0,3g/5 ml	5	230 °C 48 h	9-14 nm	[a]V_4O_7 90% + VO_2 10%
0.45	0.75	0.25	90	1 N	4→2.64	230 °C 48 h	2μm	VO_2(M) 100% **[27]**
0.225	0.375	0.125	95	1 N 12 ml	5.8→7.4	230 °C 48 h	20→100 nm	VO_2(M) 64% +VO_2(B) 36% **[27]**
0.225	0.375	0.125	100	1 N 13	7.8→7.1	220 °C 48 h	20→50 nm	VO_2(M) 14% +VO_2(B) 86% **[27]**
V_2O_5(g)	Glucose (g)	H_2O (ml)	reaction condition			Product		Morphology
0.91	0.198	30	180°C 12h			$V_3O_7{\cdot}H_2O$ and VO_2(B)		Long and short nanobelts **[28]**
0.91	1.60	30	180°C 12h			VO_2(B) and carbon		Nanosheets and carbon sphere **[28]**

Results and discussion

TEM measurements

The morphology of the samples was studied by transmission electron microscopy (TEM). The images of rGO reveal that graphene sheets were fully exfoliated **(Fig. 2(a))**. Interestingly, thin graphene flakes with large dimensions were observed as well as the thickness can be estimated to be few nanometers. **Fig. 2(b)** shows a typical panoramic TEM image of the VO-NPs film. It is clear that the geometrical shape of the vanadium oxide nanostructures is a belt with a uniform size distribution. The length and width of vanadium oxides nanobelts with very smooth and flat surfaces are 1 μm and about 9-14 nm, respectively. The TEM image in **Fig. 2(c)** confirms rod-shaped morphology of VO-NPs and show an important modification on the morphology of these nanostructures were prepared in presence of graphene nanosheets.

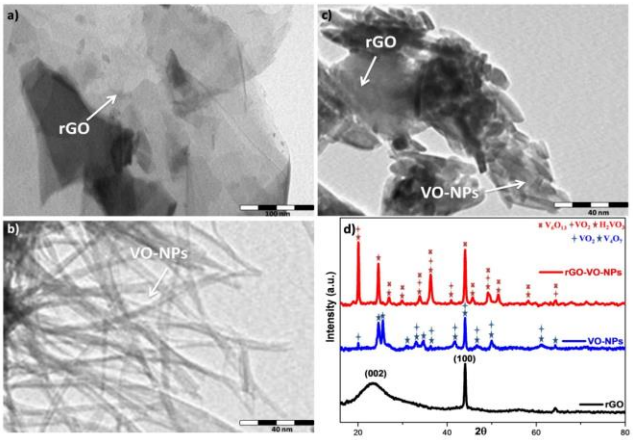

Fig. 2. (a), (b) and (c) TEM images of rGO, VO-NPs nanobelts and VO-NPs/rGO nanocomposite respectively.(d) X-rays diffraction (XRD) patterns of rGO, VO-NPs and VO-NPs/rGO nanocomposite.

The length and width of vanadium oxides nanorods with very smooth and flat surfaces are 100 nm and about 9 nm, respectively. These results confirm the serious

effect of graphene sheets on the growth of vanadium oxide nanostructures. Hence, the TEM images **(Figs. 2(a), 2(b) and 2(c))** confirm that vanadium oxides nanobelts were efficiently grown and transformed to nanorods like shape in the presence of graphene sheets.

X-ray diffraction

X-ray diffraction (XRD) patterns were used to investigate the phases and structures of rGO, VO-NPs and VO-NPs/rGO nanocomposite **(Fig. 2(d)).** The XRD pattern of rGO has two principal peaks: the first at 2θ = 23.5° confirming that GO was completely reduced by hydrazine solution **[24]** and the second peak located at about 2θ = 43° is associated to the (100) plane of the hexagonal carbon structure **[29]**. The XRD pattern of the as-prepared vanadium oxide nanoparticles revealed the existence of the two phases tetravanadium septoxide (V_4O_7) and vanadium dioxide (VO_2). The X-ray pattern For V_4O_7 corresponds to the the Triclinic crystalline phase, this is compatible with the standard value of ICDD card N° 1008024 already described in the literature (Space group 2 : A^{-1}, a = 5.456640 $\AA$, b = 6.941393 $\AA$ and c = 12.139513 $\AA$; α = 95.099998 β = 122.599998 and γ = 109.250000). Furthermore, the diffraction peaks of VO_2 can be perfectly indexed to the Monoclinic (b) crystalline phase (ICDD card N° 9009089, Space group 14 : P121/c1, a = 5.849727 $\AA$, b = 4.600944 $\AA$, c = 5.474888 $\AA$ and β = 122.599998). This revealing that the V^{5+} ions in V_2O_5 have been reduced to V^{4+} ions by the hydrazine in the reaction. No peaks of any other phases or impurities were detected in the spectra, which mean that the products are mainly composed of vanadium oxides nanoparticles. The plot in **(Figs. 3(a) and 3(b))** present an estimation of these VO_2 and V_4O_7 NPs size calculated using Hall method where the obtained size average was found to be 94 (93) and 96 (56) respectively.

Fig. 3(f) shows that the percentage of V_4O_7 was (90%) while the one of VO_2 was (10%). Furthermore, The overall elements, coordinates and occupations are summarized in the **Table2**.

The XRD pattern of the nanocomposite **(Fig. 2(d))** shows the existence of three phases, Duttonite (H_2VO_3), vanadium dioxide (VO_2) and hexavanadium tridecaoxide (V_6O_{13}). For H_2VO_3 the diffraction peaks can be readily indexed to the Monoclinic (b) crystalline phase, this is compatible with the standard value of ICDD card N° 9011014 already described in the literature (Space group 15 : I12/c1, a = 8.8268 $\AA$, b = 3.9620 $\AA$, c = 5.9781 $\AA$ and β = 90.6700). In addition, the diffraction peaks of VO_2 can be perfectly indexed to the Orthorhombic crystalline phase (ICDD card N° 9000071, Space group 62: Pbnm, a = 5.0077 $\AA$ b = 9.3563 $\AA$ and c = 2.8964 $\AA$ (α= 90.0000 β = 90.0000 γ = 90.0000).

Table 2. The overall elements, coordinates and occupations of VO-NPs.

Element	x	y	Z	Occupation
		VO_2		
V_1(V)	0.242	0.975	0.025	1
O_1(O)	0.100	0.210	0.200	1
O_2(O)	0.39	0.690	0.290	1
		V_4O_7		
V_1(V)	0.214	0.146	0.063	1
V_2(V)	0.223	0.655	0.067	1
V_3(V)	0.682	0.440	0.199	1
V_4(V)	0.687	0.941	0.202	1
O_1(O)	0.101	0.857	0.010	1
O_2(O)	0.586	0.796	0.054	1
O_3(O)	0.854	0.493	0.084	1
O_4(O)	0.327	0.436	0.137	1
O_5(O)	0.525	0.143	0.164	1
O_6(O)	0.031	0.064	0.198	1
O_7(O)	0.2956	0.792	0.224	1

In the case of V_6O_{13} the diffraction peaks can be readily indexed to the Monoclinic (b) crystalline phase (ICDD card N° 2104009, Space group 7 : P1c1, a = 10.0764 $\AA$, b = 3.7161 $\AA$ and c = 11.9817 $\AA$ (α = 90.0000 β = 100.9140 γ = 90.0000). Moreover, the plot in **Fig. 3(c), (d)** and **(e)** present an estimation of these H_2VO_3, VO_2 and V_6O_{13} NPs size calculated using Hall method where the obtained size average was found to be 264 (141), 397

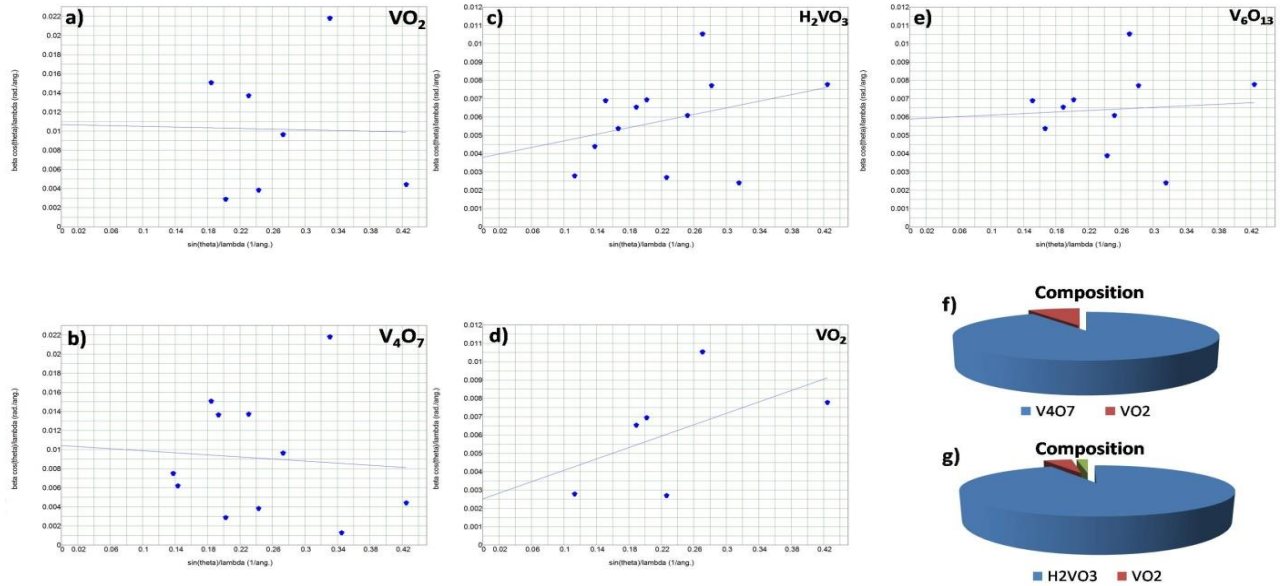

Fig. 3. (a) and (b) Size estimation in VO-NPs of VO_2 and V_4O_7 respectively, (c), (d) and (e) Size estimation in VO-NPs/rGO nanocomposite (f) and (g) Phases percentage of vanadium oxide nanostructures in VO-NPs nanobelts and VO-NPs/rGO nanocomposite respectively..

(489) and 170 (73) respectively. **Fig. 3(g)** show that the percentage of H_2VO_3, VO_2 and V_6O_{13} were (93%) (4.6%) and (2.4%) respectively. In addition, the overall elements, coordinated and occupations are summarized in **Table 3**.

These results revealed the existence of two phases of VO-NPs while graphene sheets caused a change in the crystallinity of these nanostructures by forming three phases which is in good agreement with the TEM observations.

Table 3. The overall elements, coordinates and occupations of VO-NPs/rGO nanocomposite.

Element	x	y	z	Occupation
		VO_2		
V_1(V)	0.088	0.143	0.250	1
O_1(O)	0.106	-0.235	0.250	1
O_2(O)	-0.227	-0.013	0.250	1
		H_2VO_3		
V_1(V)	0.000	0.336	0.250	1
O_1(O)	0.000	0.754	0.250	1
O_2(O)	0.150	0.250	0.500	1
O_3(O)	0.507	0.282	0.454	1
		V_6O_{13}		
V_1(V)	-0.006	0.297	0.346	1
V_2(V)	-0.003	0.236	0.642	1
V_3(V)	0.360	0.250	0.417	1
V_4(V)	0.632	0.248	0.591	1
V_5(V)	0.364	0.249	0.719	1
V_6(V)	0.631	0.252	0.289	1
O_1(O)	-0.003	0.256	0.184	1
O_2(O)	0.385	0.249	0.886	1
O_3(O)	0.407	0.252	0.254	1
O_4(O)	-0.003	0.240	0.502	1
O_5(O)	0.192	0.252	0.387	1
O_6(O)	0.197	0.246	0.682	1
O_7(O)	0.404	0.251	0.565	1
O_8(O)	-0.004	0.241	0.829	1
O_9(O)	0.609	0.251	0.122	1
O_{10}(O)	0.588	0.248	0.752	1
O_{11}(O)	0.799	0.247	0.617	1
O_{12}(O)	0.799	0.254	0.322	1
O_{13}(O)	0.589	0.251	0.442	1

Raman spectroscopy

Raman spectroscopy is a powerful technique to characterize reduction and exfoliation of layers. The Raman spectra of the of rGO, VO-NPs and VO-NPs/rGO nanocomposites prepared in films form are shown in **Fig. 4**. The spectrum of the rGO displays two main bands; the first one G band located at 1600 cm^{-1} arises from the stretching of C-C bond in graphitic materials which is due to the first-order scattering of the E_{2g} phonons at the Γ -point. The second one D band at 1330 cm^{-1} arising from the breathing mode of k-point phonons of A_{1g} symmetry **[24]**. In addition, G band represent the in-plane stretching of ordered sp^2 bonded carbon atoms while D band is ascribed to defects such as the density of impurity, disordered carbon and oxygen -containing functional groups on graphene **[30, 31]**. In addition, rGO spectrum exhibits another broad band around 2600-2800 cm^{-1} corresponding to 2D band is a second -order two-phonon lattice process which is referred to the rGO number of layers **[31]**. The intensity ratio of D to G bands I_D/I_G corresponding to the sp^3 to sp^2 hybridization, for the VO-NPs/rGO nanocomposite intensity ratio (1.38) decreased. This could be due to the decrease in sp^3 groups corresponding to defects produced after hydrazine treatment of GO.

In addition, this behavior confirms the reduction of defects in rGO nanolayers after the interaction with the VO-NPs nanobelts, leading to an increase of graphitic domain created in VO-NPs/rGO nanocomposite.

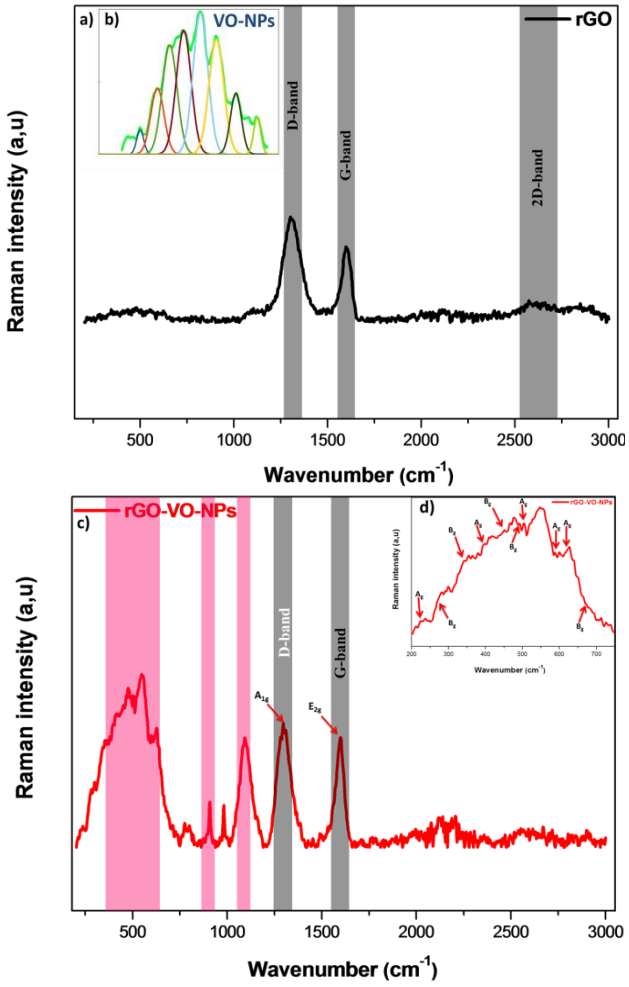

Fig. 4. (a) Raman spectra of the rGO. (b) inset zoom VO-NPs nanobelts. (c) VO-NPs/rGO nanocomposite; (d) inset zoom low frequency region from 250 to 750 cm_{-1} of VO-NPs/rGO nanocomposite.

The sample of VO-NPs prepared by hydrothermal synthesis at 230 ˚C for 2 days was investigated by Raman spectroscopy **(Fig. 4(b))**. In this sample, the spectrum of VO-NPs displays a series of Raman band corresponds to the various vibrations of V-O type. The spectrum showed the peak at 982 cm^{-1} could be attributed to the V=O stretching vibrations **[32]**. Furthermore, the peak at 688 cm^{-1} corresponds to the doubly coordinated oxygen (V_2-O) stretching mode, which is due to corner-shared oxygen common to two pyramids **[33, 34]**. The peak at 524 cm^{-1} is attributed to the triply coordinated oxygen (V_3-O) stretching mode of edge-shared oxygen in common with three pyramids **[33, 34]**.

In addition, the peaks of weaker intensity which could be attributed to V-O-V bridging modes were observed at 407 cm^{-1} and 485 cm^{-1} **[32, 35]**. The two peaks located at 339 and 618 cm^{-1} are associated to the vibrational modes

B_g and A_g respectively **[36]**. Finally, the Raman spectrum shows the existence of a band at 287 cm^{-1} which could be attributed to V-O-V in the bending mode **[32]**.

The Raman spectrum of the nanocomposite prepared from rGO and VO-NPs is shown in **Fig. 4(c)**. The new two peaks appearing at 818 and 907 cm^{-1} are assigned to the B_g vibrational mode and the presence of hydrated VO-NPs nanords. In addition, the two peaks located at 998 and 1096 cm^{-1} becomes very intense compared with vanadium oxide nanobelts peaks, these results may be due to the change of size and or shape of VO-NPs which confirms the TEM observations and the results obtained from X-ray diffractions. Furthermore, the Raman band in the range of 200- 1000 cm^{-1} becomes more intense, which indicated a good interaction between vanadium oxide nanobelts and rGO nanosheets. Below 750 cm^{-1} **(Fig. 4(d))**, the vibrational Raman active mode of VO-NPs/rGO can be described in terms of vanadium-oxygen stretching modes, vanadium-oxygen-vanadium bending vibrations, and translational modes **[33, 35–37]**. Therefore, the Raman results are consistent with the formation of VO-NPs/rGO nanocomposite.

UV-vis spectroscopy

Ultraviolet-visible absorbance spectra of rGO, VO-NPs and VO-NPs/rGO nanocomposite are shown in **Fig. 5**. The UV-Vis absorption spectrum of reduced graphene oxide shows a strong absorption peak at 270 nm in the UV region. Which is mainly associated to n-π^* transition of C-O bonds now embedded by exfoliation and intercalation on the graphene sheets **[24]**. Compared with graphene oxide (GO), the red shift from 230 to 270 nm is due to the electronic configuration of graphene after the reduction of graphene oxide **[24]**. The transformation of GO in our sample is confirmed by the disappearance of C-C band centered at around 230 nm and its shifting to 270 nm upon reduction likely due to the decrease in the concentration of carboxyl groups indicating that the electronic conjugation within the reduced graphene sheets was revived upon reduction of graphene oxide **[24]**.

The UV-Vis absorption spectrum of VO-NPs nanobelts **(Fig. 5b)** has two bands located at around 253 nm and 370 nm, the first could be assigned to charge transfer transition, involving oxygen and vanadium (IV) in tetrahedral coordination, present in isolated species **[38, 39]**. The second broad band at 370 nm is attributed to octahedral V^{4+} specie [**36**]. Moreover, the Uv-Vis spectrum of VO-NPs/rGO nanocomposite absorbance shown in **(Fig. 5(c))** presents the existence of four bands. The intense one is located at 273 nm can be attributed to the absorption of graphene layers. The second one located at 253 nm is due to the absorption of VO-NPs. Moreover, the band at 490 nm can be attributed to the electron transfer from oxygen atoms to vanadium in octahedral coordination **[39]**. Indeed, the origin of this change of spectral band position was suggested to be the contribution of a quantum size effect in the VO-NPs **[39, 40]**. Finally, the band at 690 nm is attributed to d-d transition of V^{4+} [**41**]. According to the works by Luan *et al.*, Dutoit *et al.* [**42, 43**] and also Golinska *et al.* [**44**].

The gap energy from Uv-visible spectra absorbance can be determined at the tangent to the absorption front, and the width of the band gap is strongly dependent on the conjugation length. The band gap of the VO-NPs/rGO nanorods nanocomposite was found to be 2.57 eV which can be attributed to direct transition from occupied 2p bands of oxygen to unoccupied 3d bands of vanadium [**45, 46**]. On one hand, the optical band gap of bulk monoclinic VO2 is Eg = 0.7 eV. On the other hand, Liu et al and Wang reported that the band gap of vanadium oxide nanosheets were 1.87 [**47**] and 2.1 eV [**48**], respectively. Our results show a higher band gap. This increment could be attributed partially to dimensional confinement effects of the nanorods [**49, 50**]. Furthermore, Compared with vanadium oxide nanobelts (Eg = 3.33 eV), in the nanocomposites the gap energy decreases after the introduction of graphene nanosheets to (Eg = 2.57 eV) confirming that vanadium oxide nanobelts were transformed to nanorods like shape after incorporation with graphene nanosheets.

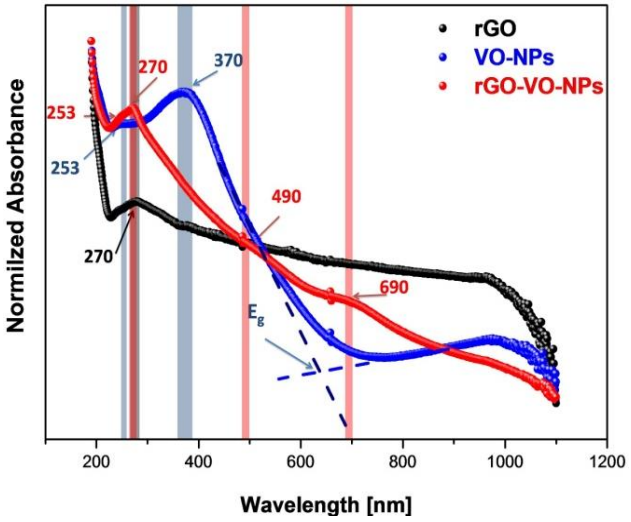

Fig. 5. Uv-Vis optical absorbance spectra: (a) rGO, (b) VO-NPs nanobelts and (c) VO-NPs/rGO nanocomposite.

Conclusion

To summarize, the present study demonstrates important interactions and effects of the growth of vanadium oxide on graphene layers. It is revealing that vanadium oxide nanobelts were efficiently grown and had nanorods like shape in the presence of graphene. In addition, the obtained phases without graphene were different to the ones which were obtained in its presence. This is clearly showing the strong effect of rGO layers on the growth of vanadium oxide nanostructures which leads to a change in the form, the shape and the phase. The previous outcomes were confirmed by showing the formation of new vibrational bonds which assisted to the understanding of the growth mechanism. Furthermore, it is revealing an important effect on the optical properties of this hybrid material. Hence, the importance of this study is focused on its offering of information which may assist to control the preparation of this hybrids and modulate their properties to enhance their efficiency then improve the performance of their applications.

Acknowledgements

Special thanks to the Innovation city of USMBA (Morocco), Abdus Salam International Centre for Theoretical Physics (Trieste-Italy), Nanosciences African Network, University of South Africa Department of Physics, iThemba Labs (South Africa), African Laser Center and Africa Graphene Center.

References

1. Andre Konstantin, G.; Konstantin Sergeevich, N; *Nat. Mater*., **2007**, *6*, 183. **DOI:**10.1038/nmat1849
2. Francesco, B.; Zhipei, S.; Tawfique, H.; Andrea, C. F; *Nat. Photon*, **2010,** *4*, 611. **DOI:**10.1038/nphoton.2010.186
3. Andrea, C. F.; Francesco, B.; and al; *Nanoscale*, **2015**, *7*, 4598. **DOI:**10.1039/C4NR01600A
4. Jacques, L; *Materials*, **2010**, *3*, 4175. **DOI:**10.3390/ma3084175
5. Marcos, F. G.; Arturo, M. A.; Jonathan, H.; José, A. R; *Chem. Rev*., **2004**, *104*, 4063. **DOI:**10.1021/cr030032f
6. Shidong, Ji.; Yangang, Z.; Feng, Z.; Ping, J; *J. Cryst. Growth*., **2010**, *312*, 282. **DOI:**10.1016/j.jcrysgro.2009.10.026
7. Nagaraju, G.; Ashoka, S; *Materials Characterization*, **2012**, *68*, 58. **DOI:**10.1016/j.matchar.2012.03.010
8. Troy, D. M.; Ivan, P. P.; Martyn, E. P.; David, S.; Dimitra, V; *Chemistry of Materials*, **2004**, *16*, 744. **DOI:**10.1021/cm034905y
9. Ningyi, Y.; Jinhua, L.; Chenglu, L; *Appl. Surf. Sci*., **2002**, *191*, 176. **DOI:**10.1016/S0169-4332(02)00180-0
10. Serena, A Corr.; Madeleine, G.; Yifeng, S.; Kevin, R. H.; Galen, D. S.; Ram, S; *J. Mater. Chem.*, **2009**, *19*, 4362. **DOI:**10.1039/B900982E
11. Zifei, P.; Wei, J.; Heng, L; *J. Phys. Chem. C*, **2007**, *111*, 1119. **DOI:**10.1021/jp066342u
12. Kim, D. H.; Kwok, H. S; *Appl. Phys. Lett.*, **1994**, *65*, 3188. **DOI:**10.1063/1.112476
13. Mingxian, L.; Lihua, G.; Wei, X.; Fengqi, Z.; Xuezhong, F.; Dazhang, Z.; Zijie, X.; Zhixian, H.; Longwu, C; *Energy Fuels*, **2013**, *27*, 1168. **DOI:**10.1021/ef302028j
14. Sharon, M.; Sharon, M.; Shinohara, H.; Tiwari, A.; (Eds), In the Graphene: An Introduction to the Fundamentals and Industrial Applications, Wiley, USA, **2015**.
15. Sanjaya, D. P.; Anjalee, D. L.; Nour, N.; John, P. F.; Yves, J. C.; Kenneth, J. B. Jr; *J. Power Sources*, **2013**, *230*, 130. **DOI:**10.1016/j.jpowsour.2012.11.118
16. Xiao, H.; Xiaoying, Q.; Freddy, B.; Hua, Z; *Chem. Soc. Rev*., **2012**, *41*, 666. **DOI:**10.1039/c1cs15078b
17. Minghui, L.; Linjie, Z; *J. Mater. Chem*., **2009**, *19*, 5871. **DOI:**10.1039/B901551E
18. Hongbin, Z.; Lanying, P.; Siyi, X.; Jun, L.; Jiaqiang, X; *J. Power Sources*, **2013**, *222*, 21. **DOI:**10.1016/j.jpowsour.2012.08.036
19. Jung, Woo. L.; Soo, Yeon. L.; Hyung, Mo. J.; Tae, Hoon. H.; Jeung, Ku. K.; Jang, Wook. C; *Energy Environ. Sci*., **2012**, *5*, 9889. **DOI:**10.1039/C2EE22004K
20. Huanwen, W.; Huan, Y.; Xiao, C.; Xuefeng, W; *Journal of Materials Chemistry A*, **2014**, *2*, 1165. **DOI:**10.1039/C3TA13932H
21. Nethravathi, C.; Catherine, R. R.; Michael, R.; Ujjal, K. G.; Xi, W.; Dmitri, G.; Yoshio, B; *Appl. Mater. Interfaces*, **2013**, *5*, 2708. **DOI:**10.1021/am400202v
22. Yi, S.; Shulei, C.; Jia-Zhao, W.; David, W.; Hui-Jun, L.; Hua-Kun, L.; Yuping, W; *J. Mater. Chem*., **2012**, *22*, 16465. **DOI:**10.1039/c2jm32649c
23. Chao, Z.; Jiazhao, W.; Zhixin, C.; Huakun, L; *J. Phys. Chem. C*., **2011**, *115*, 25115. **DOI**:10.1021/jp2061128
24. Mohammed, K.; Ulrich, B.; Mimouna, B.; Malik, M; *Graphene*, **2014**, *3*, 7. **DOI:**10.4236/graphene.2014.32002
25. Mohammed, K.; Mimouna, B.; Malik, M; *Opt. Mater*., **2014**, *36*, 27. **DOI:**10.1016/j.optmat.2013.07.004
26. Chengyi, H.; Qinghong, Z.; Meifang, Z.; Yaogang, L.; Hongzhi, W.; *Carbon*, **2011**, *49*, 47. **DOI:**10.1016/j.carbon.2010.08.040
27. Jung-Ho, S.; Jiang, W.; David, C; Guozhong, C; Younan, Xia; *Chem. Mater*., **2010**, *22*, 3043. **DOI:** 10.1021/cm903727u
28. Yifu, Z.; Meijuan, F.; Min, Z.; Chi, H.; Chongxue, C.; Yuliang, C.; Guangyong, X.; Houbin, L.; Xinghai, L.; *Bull. Mater. Sci.*, **2012**, *35*, 369. **DOI:** 10.1007/s12034-012-0311-9
29. Yingqing, Z.; Fanbin, M.; Yajie, L.; Rui, Z.; Jiachun, Z.; Xiaobo, L; *Materials Letters*, **2011**, *65*, 1737. **DOI:**10.1016/j.matlet.2011.03.019
30. Anindya, D.; Biswanath, C.; Sood, A. K; *The Bulletin of Materials Science*, **2008**, *31*, 579. **DOI:**10.1007/s12034-008-0090-5
31. Pimenta, M. A.; Dresselhaus, G.; Dresselhaus, M. S.; Canado, L. G.; Jorio, A.; Saito, R; *Phys. Chem. Chem. Phys*., **2007**, *9*, 1276. **DOI:**10.1039/B613962K
32. Rui, L.; Chun-Yan, L; *Materials Research Bulletin*, **2010**, *45*, 688. **DOI:**10.1016/j.materresbull.2010.02.021
33. Faggio, G.; Modafferi, V.; Panzera, G.; Alfieri, D.; Saveria, S; *J. Raman Spectrosc.*, **2012**, *43*, 761. **DOI:**10.1002/jrs.3089
34. Baddour-Hadjean, R.; Asma, M.; Pereira-Ramos, J. P.; *J. Raman Spectrosc.*, **2012**, *43*, 153. **DOI:**10.1002/jrs.2984
35. Petrov, G. I.; Vladislav, Y.; Squier; J; *Appl. Phys. Lett.*, **2002**, *81*, 1023. **DOI:**10.1063/1.112476
36. Peter, S.; *Physica B*, **2002**, *316*, 600. **DOI:**10.1016/S0921-4526(02)00584-7
37. Wei-Chuan, F; *J. Phys. Chem. C*, **2008**, *112*, 11552. **DOI:**10.1021/jp8011602
38. Viviana, M.; Elsa M. Farfán, T.; Juan C, G.; Edgardo L, S; *Applied Catalysis A*: General, **2006**, *312*, 134. **DOI:**10.1016/j.apcata.2006.06.042
39. Jun, L.; Dongfeng, X; *Nanoscale Res. Lett.;* **2010**, *5*, 1619. **DOI:**10.1007/s11671-010-9685-z
40. Chenglin, Y.; Dongfeng, X; Adv. Mater., **2008**, *20*, 1055. **DOI:**10.1002/adma.200701752
41. Xing, C.; Wenguang, Z.; Feng, W.; Jie, X; *Journal of Natural Gas Chemistry*, **2012**, *21*, 481. **DOI:**10.1016/S1003-9953(11)60394-0
42. Zhaohua, L.; Jie, X.; Heyong, H.; Jacek, K.; Larry, Kevan; *J. Phys. Chem. A*, **1996**, *100*, 19595. **DOI:**10.1021/jp962353j
43. Dutoit, D. C. M.; Schneider, M.; Fabrizioli, P.; Baiker, A.; *Chem. Mater*., **1996**, *8*, 734. **DOI:**10.1021/cm9504293
44. *Golinska, H.; Decyk, P.; Ziolek, M.; Kujawa, J.; Filipek, E; Catalysis Today*, ***2009***, *142*, *175*. **DOI:**10.1016/j.cattod.2008.10.044
45. Sukanta, D.; Ashis, D.; Subodh Kumar, D; *Solid State Commun*, **2006**, *137*, 662. **DOI:**10.1016/j.ssc.2006.01.027
46. Sukanta, D.; Arup, D.; Subodh Kumar, D; *J. Phys. Chem. Solids*, **2007**, *68*, 66. **DOI:**10.1016/j.jpcs.2006.09.001
47. Liang, L.; Tao, Y.; Xiaogang, T.; Qinghua, L.; Zhiqiang, W.; Dacheng, S.; Zhihu, S.; Shiqiang, W.; Yi, X; *Small*, **2012**, *8*, 3752. **DOI:**10.1002/smll.201201552
48. Ying-Ting, W.; Chun-Hua, C; *Inorg. Chem*., **2013**, *52*, 2550. **DOI:**10.1021/ic302562j
49. Yuquan, W.; Zhengjun, Z.; Yu, Z.; Zhengcao L.; Robert, V.; Lijie, C.; Pulickel Madhavapanicker, A; *ACS Nano*, **2008**, *2*, 1492. **DOI:**10.1021/nn800223s
50. Jun, L.; Dongfeng, X; *Adv. Mater*, **2008**, *20*, 2622. **DOI:** 10.1002/adma.200800208